International Journal of Applied Mathematics, Sciences, and Technology for National Defense
Volume 3, Issue 2, 103-116
e_ISSN: 2985-9352, p_ISSN: 2986-0776
https://www.journal.foundae.com/index.php/JAS-ND
DOI : https://doi.org/10.58524/app.sci.def.v3i2.841

Shielding innovation for health security: A PHITS-based optimization of Portland material for proton therapy

Damar Adhiwidya Suyanto
Indonesia Defense University
INDONESIA

Aditya Tri Oktaviana*
Indonesia Defense University
INDONESIA

Mikael Syväjärvi
Alminica AB, Ulrika
SWEDEN

Yohannes Sardjono
Badan Riset dan Inovasi Nasional
INDONESIA

Gede Sustresna Wijaya
Badan Riset dan Inovasi Nasional
INDONESIA

Isman Mulyadi Triatmoko
Badan Riset dan Inovasi Nasional
INDONESIA

Article Info

Article history:

Received: May 22, 2025
Revised: July 29, 2025
Accepted: August 11, 2025
Published: August 30, 2025

Keywords:

Cyclotron
PHITS
Portland material
Proton therapy
Radiation attenuation

Abstract

Proton therapy is an advanced treatment method for cancer that uses protons to irradiate tumors with high precision. However, the high energy of protons requires effective shielding to protect the surrounding environment and personnel from radiation exposure. In this research, the radiation shielding performance of Portland material was evaluated using the PHITS version 3.351 simulation software. The study focuses on assessing the attenuation of radiation within the cyclotron room under various operational conditions. The effectiveness of radiation shielding made from Portland material in a 230 MeV, 300 NA cyclotron room for a proton therapy facility was investigated. The results from PHITS simulations provide insights into the potential of Portland material in reducing radiation levels in proton therapy rooms, contributing to the safety and efficiency of such facilities. This analysis is essential for optimizing shielding design and ensuring compliance with safety regulations in proton therapy facilities.

To cite this article: Suyanto, D. A., Oktaviana, A. T., Syväjärvi, M., Sardjono, Y., Wijaya, G. S., & Triatmoko, I. M. (2025). Shielding innovation for health security: A PHITS-based optimization of Portland material for proton therapy. *International Journal of Applied Mathematics, Sciences, and Technology for National Defense,* 3(2), 103-116

INTRODUCTION

Radiation shielding is a critical component in defense applications, providing protection for personnel and sensitive equipment against neutron and gamma radiation in nuclear-powered submarines (Yamaji et al., 1994; Reistad et al., 2006; Wan et al., 2017), spacecraft (El-Genk, 2009; Durante et al., 2011; Caffrey, 2017), and high-energy particle accelerator facilities employed in defense research (Ruth, 2009; Giménez et al., 2018; Saadi et al., 2019). The design of shielding systems for naval reactors and satellite-based nuclear platforms is increasingly reliant on advanced computational simulations to mitigate secondary radiation, a methodological approach comparable to that adopted in precision-driven radiation therapy facilities (Chen et al., 2019). Progress in shielding materials and modeling techniques thus demonstrates clear dual-use potential, simultaneously strengthening civilian medical infrastructure and reinforcing military radiation protection protocols (Till & Grogan, 2008).

In the medical domain, shielding effectiveness is particularly significant in proton therapy facilities, where Portland cement remains a widely utilized structural material to limit radiation exposure for both patients and healthcare personnel. Recent advancements in computational

***Corresponding Author:**
Aditya Tri Oktaviana, Indonesia Defense University, Indonesia, Email: oktavianaadit@gmail.com

transport modeling, notably through the Particle and Heavy Ion Transport code System (PHITS), further emphasize the importance of rigorous shielding design in optimizing both safety and clinical efficacy in proton therapy

Proton radiation shielding is a complex but crucial discipline that involves understanding how protons interact with matter to design effective barriers against both the primary beam and the more challenging secondary radiation. When high-energy protons collide with a shielding material, they can ionize and excite atoms, but more significantly, they can also cause nuclear reactions that produce a cascade of penetrating secondary particles, including neutrons, gamma rays, and other subatomic particles. The cutting edge of Portland cement research is primarily focused on creating sustainable, high-performance, and "smart" materials to address both environmental concerns and modern construction demands. To combat the significant carbon footprint of traditional cement, innovations center on using Supplementary Cementitious Materials (SCMs) like calcined clay in blends such as LC3 to reduce the energy-intensive clinker content, alongside the development of carbon capture technologies and alternative raw material sources. The effectiveness of radiation shielding in proton therapy facilities, particularly using Portland cement as a primary construction material, is critical in minimizing radiation exposure for both patients and healthcare workers. Recent advancements in computational simulations, particularly through the use of the Particle and Heavy Ion Transport code System (PHITS), underscore the significance of shielding design and its modeling for proton therapies (Krishnaraja & Guru, 2021).

Proton therapy benefits from a unique advantage over conventional photon therapies due to the distinct Bragg peak phenomenon, which localizes dose delivery to tumors while sparing surrounding healthy tissues (Depuydt, 2018). However, this advantage necessitates robust shielding practices to protect against secondary radiation, including neutrons and gammas produced during treatment (Matsumoto et al., 2016). Studies have shown that secondary neutron doses can lead to significant exposure for personnel if shielding is not adequately designed (Gultom. 2024). Monte Carlo simulation tools, such as PHITS, are instrumental in optimizing this aspect by enabling researchers to evaluate designs comprehensively, including radiation interactions with different materials.

Several studies have demonstrated the comparative effectiveness of proton versus photon therapy. Notably, Baumann et al. conducted a study highlighting the lower observed toxicity in patients undergoing proton therapy relative to those receiving photon therapy as part of concurrent chemoradiotherapy for locally advanced cancer, suggesting that the higher upfront cost of proton therapy may be offset by cost savings from reduced hospitalizations and enhanced productivity from patients and caregivers (Baumann et al., 2020). Furthermore, a systematic review by Chen et al. underscored the benefits of modern delivery techniques such as intensity-modulated proton therapy (IMPT), which effectively mitigates the exposure of normal tissues while achieving accurate tumor targeting, which is pivotal for higher clinical outcomes (Chen et al., 2023).

Cost-effectiveness analyses have also positioned proton therapy favorably within the landscape of cancer treatments. Brodin et al. discussed the potential for proton therapy to offer individualized quality of life benefits and reduced rates of emergency room visits, indicating that these reductions in unplanned hospitalizations may contribute significantly to the overall cost-effectiveness of proton therapy for patients with oropharyngeal cancer (Brodin et al., 2021). In a broader context. evaluated the economic implications of proton therapy for head and neck cancers, reinforcing that while the upfront costs are significant, the long-term value gained through minimized treatment-related complications can provide substantial overall cost savings (Huang et al., 2021).

Moreover, recent investigations into biologically enhanced therapies are gaining traction, suggesting an adjunctive approach using boron compounds. For instance, Tabbakh et al. highlighted the potential for boron nanoparticles to enhance proton therapy's efficacy, indicating that the nuclear interactions facilitated by these compounds could significantly increase therapeutic outcomes (Tabbakh et al., 2022). Similarly, Popov et al. explored the molecular mechanisms by which boron compounds could sensitize tumor cells to proton therapy, presenting a promising avenue for further research (Popov et al., 2024).

The exploration of advanced simulation tools and techniques further highlights the evolving landscape of proton therapy. Goitein emphasized the necessity of accurate proton range estimation

to mitigate uncertainties in dose delivery, proposing the use of deep learning frameworks for generating synthetic dose-weighted linear energy transfer (LET) maps that could enhance treatment planning accuracy (Goitein, 1985). Such advancements are crucial as they improve the precision of targeting, a hallmark of proton therapy's clinical effectiveness.

In conclusion, literature underscores a robust optimism surrounding proton therapy characterized by its clinical efficacy, potential for reduced toxicity, and advancements in complementary technologies. The continued research and development in this field not only bolster therapeutic outcomes but also provide a pathway towards enhanced quality of life for patients undergoing cancer treatment. While the initial context explains the general importance of proton therapy and shielding, it lacks a specific, problem-driven rationale for this particular study. The revised introduction will now highlight the critical gap: that despite the widespread use of Portland cement in these facilities, there is a lack of detailed, high-fidelity simulation data for its performance against the specific secondary neutron spectra produced by a high-energy, high-current cyclotron. This study is therefore motivated by the need to fill this knowledge gap, providing precise, validated data through PHITS simulations. This will not only ensure a more accurate and cost-effective shielding design but also contribute to an improved safety protocol, moving beyond traditional, conservative shielding assumptions towards an optimized, data-driven approach tailored to the unique output of a 230 MeV cyclotron. By framing the study as a response to this specific technical challenge, the paper's contribution becomes immediately clear and relevant.

METHOD

Computational data and statistical analysis were performed using a MacBook Pro with an M1 Pro chip (Apple Inc., Cupertino, CA, USA) running the macOS Monterey operating system (version 12.0.1) and R software (version 4.1.2; R Foundation for Statistical Computing, Vienna, Austria). The simulations were conducted using the PHITS simulation program, version 3.51, which is essential for modeling particle transport and radiation shielding. Additional tools utilized in this research include Microsoft Word 2021 and Microsoft Excel 2021 for documentation and data analysis. The PHITSPAD_launch and EPSPDF programs were used for launching and processing simulations, while Ghostscript was employed for handling PDF file conversions.

Cyclotron 230 MeV Design

In this study, the S2C2 cyclotron with an energy of 230 MeV in Figure 1 is used as the primary particle source for proton therapy simulations in a shielding room. The S2C2 cyclotron, designed to accelerate protons to an energy of 230 MeV, plays a pivotal role in delivering high-energy protons to the treatment area.

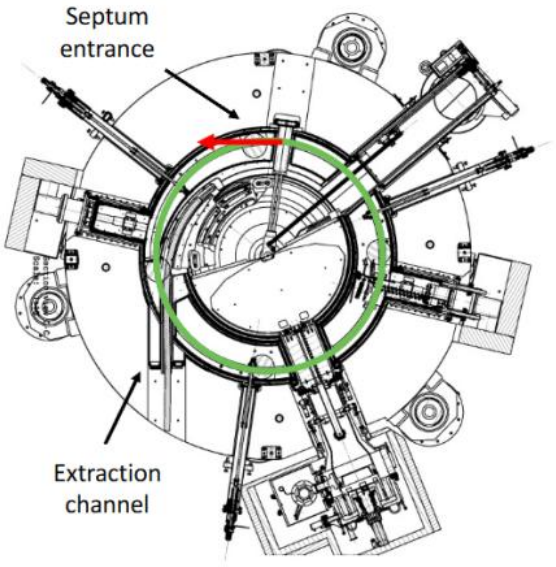

Figure 1. The illustration shows two sources of proton losses in the S2C2, simulated in BDSIM: uniformly distributed losses along the accelerator's circumference (green) and losses at the septum (red) (Ramoisiaux et al., 2023).

For the purpose of this research, the cyclotron is modeled within the simulation environment to assess its interaction with the shielding materials. The shielding room is specifically designed to protect personnel and surrounding areas from radiation exposure, and it is equipped with various protective materials to attenuate the proton beam as it moves from the cyclotron to the treatment room. The simulation takes into account the cyclotron's geometry, the proton beam extraction system, and the energy spectrum of the protons, enabling a detailed evaluation of the radiation shielding effectiveness in a proton therapy facility.

Design of Shielding Room for Proton Therapy

The design of the shielding room for proton therapy in Figure 2 consists of several key areas, each serving a specific purpose in the overall treatment process. The cyclotron room is the first component, housing the S2C2 cyclotron, where protons are accelerated to high energies before being directed towards the treatment rooms. The first treatment room, Treatment Room 1, is where the proton therapy takes place, with the proton beam delivered precisely to the tumor site for therapeutic purposes. Treatment Room 2 is designated as the patient and radiologist entry area, providing a space for patient preparation and positioning before entering Treatment Room 1. Effective shielding is incorporated into all these spaces to minimize radiation exposure to personnel and surrounding areas while ensuring the safety and efficacy of the proton therapy process.

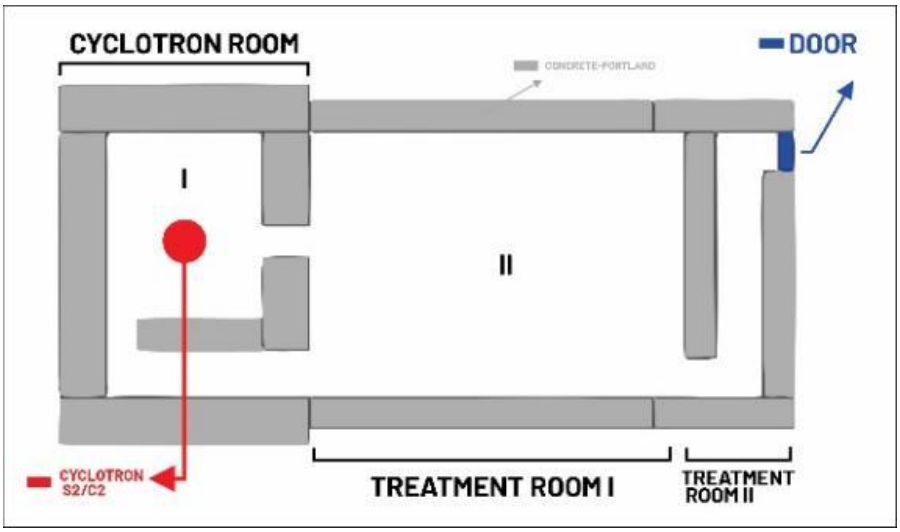

Figure 2. Design of shielding room with PHITS.

Spatial Geometry of Accelerators

The facility is divided into three distinct rooms with specific functions. The first room, measuring 9 m × 5 m × 3 m, is where the cyclotron accelerator is located. Adjacent to it is the second room, which spans 20 m × 5 m × 3 m and serves as the beam transport system area. The third room, measuring 9 m × 2 m × 3 m, acts as the entrance to the second room and provides access to the beam transport system. All three rooms are surrounded by shielding materials to ensure safety, and the entrance is equipped with a plug door made of barite concrete, which is coated with carbon steel. This design provides essential protection against radiation for both the system and its users.

The calculation of radiation doses for each wall is divided according to the numbered sections indicated in Figures 3 and 4. These figures provide a detailed breakdown of the dose distribution, allowing for a clear understanding of the shielding requirements for each specific wall in the facility (Ying et al., 2020). The numbers correspond to different areas, helping to identify the precise radiation protection measures necessary for each section (Penfold, 2022).

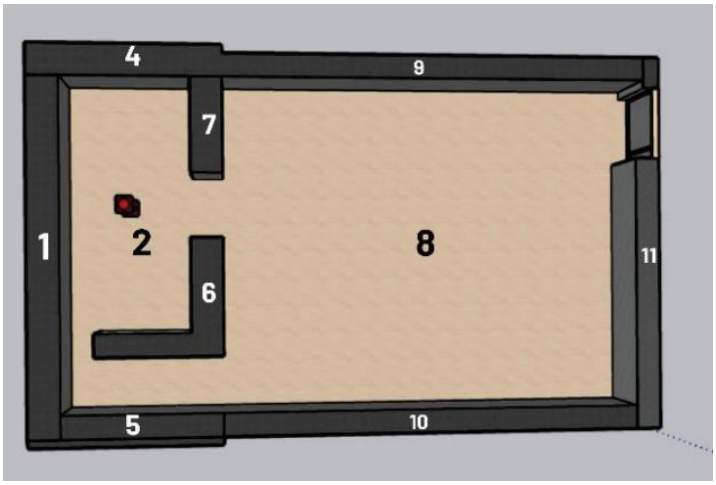

Figure 3. Room Geometry in axial view.

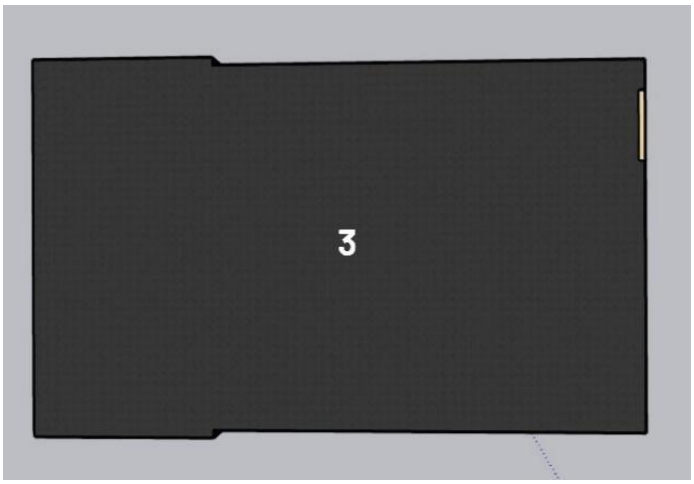

Figure 4. The roof of the shielding room.

The spatial division of the facility is outlined, focusing on the wall configuration of three primary rooms: the cyclotron room, the beam transport system room, and the treatment room. Each room plays a crucial role in the overall operation of the accelerator system. The walls are numbered to indicate their specific location and function within the facility, with careful attention given to shielding and accessibility. Below is the breakdown of each wall based on its position in the respective rooms.

1) **Wall 1**: The back of the cyclotron, serving as the rear boundary of the cyclotron room.
2) **Wall 2**: The floor of the cyclotron room, providing the foundation for the equipment within this area.
3) **Wall 3**: The roof of the entire shielding room, offering protection against radiation from above.
4) **Wall 4**: The right side of the cyclotron in the cyclotron room, marking the right boundary of the space housing the cyclotron.
5) **Wall 5**: The left side of the cyclotron in the cyclotron room, marking the left boundary of the cyclotron area.
6) **Wall 6**: The left side of the beam transport system, acting as the left boundary for the beam's pathway.
7) **Wall 7**: The right side of the beam transport system, serving as the right boundary of the beam's transport area.
8) **Wall 8**: The floor of the beam transport system room, forming the base on which the beam transport system operates.
9) **Wall 9**: The right side of the treatment room, marking the right boundary of the therapy space.
10) **Wall 10**: The left side of the treatment room, defining the left boundary of the therapy room.

11) **Wall 11**: The front of the entrance to the treatment room, allowing access to the therapy area from the main passageway.

Research Variables

This study, the research variables are the type of material and the material thickness. The type of material used is Portland cement. The composition of various shielding materials based on atomic fraction, as referenced from the *Compendium of Material Composition Data for Radiation Transport Modelling*, is shown in Table 1. These materials play a crucial role in ensuring the effectiveness of radiation shielding and contribute to accurate radiation transport modeling.

Table 1. Composition of radiation shielding materials (Detwiler. R.S, et al, 2021).

Material Component	Portland Cement (ρ = 2,35 g/cm^3)
H	16.875
C	0.142
O	56.253
Na	1.184
Mg	0.14
Al	2.135
Si	20.412
S	
K	0.566
Ca	1.867
Fe	0.426
Ba	

Analysis of Research Results

The dose rate values are derived by converting the particle flux using the multiplier 202 command, which is consistent with the ICRP 103 recommendations from 2007. The multiplier's output is in pSv and is subsequently converted to µSv." (Garg & Shrigiriwar, 2022)

The variables in this study are the type and thickness of the material. For each material, the thickness is varied to determine the dose rate that meets the regulations set by BAPETEN Regulation No. 3 of 2013. In this study, it is assumed that the general public is exposed for 2000 hours per year. The maximum dose for the general public is determined by the following equation.

$$Exposure\ time = 8\frac{hour}{day} \times 5\frac{day}{week} \times 50\frac{week}{year} = 2000\frac{hour}{year} \quad (1)$$

$$Maximum\ dose = \frac{500\ \mu Sv/year}{2000\ hour/year} = 0.25\ \mu Sv/hour \quad (2)$$

RESULTS AND DISCUSSION

The thickness and dose rate for each wall in the Portland cement shield design are listed in the Tables 2.

Table 2. Thickness and dose rate

Wall	Thickness (cm)	Proton dose rate (µSv/hour)	Neutron Dose Rate (µSv/hour)	Photon Dose Rate (µSv/hour)	Total Dose Rate (µSv/Hour)
1	190	0	$1{,}909 \times 10^{-1}$	$1{,}169 \times 10^{-2}$	$2{,}060 \times 10^{-1}$
2	200	$8{,}900 \times 10^{-3}$	$1{,}525 \times 10^{-1}$	$4{,}031 \times 10^{-3}$	$1{,}829 \times 10^{-1}$
3	150	0	$1{,}496 \times 10^{-1}$	$4{,}731 \times 10^{-3}$	$1{,}544 \times 10^{-1}$
4	220	0	$5{,}626 \times 10^{-2}$	$1{,}459 \times 10^{-3}$	$8{,}656 \times 10^{-2}$
5	170	$2{,}002 \times 10^{-5}$	$5{,}626 \times 10^{-2}$	$7{,}425 \times 10^{-3}$	$5{,}793 \times 10^{-2}$
6	350	$8{,}924 \times 10^{-5}$	$2{,}182 \times 10^{-3}$	$9{,}560 \times 10^{-4}$	$2{,}193 \times 10^{-3}$
7	350	$7{,}684 \times 10^{-5}$	$1{,}354 \times 10^{-1}$	$1{,}022 \times 10^{-3}$	$2{,}065 \times 10^{-1}$
8	200	$6{,}900 \times 10^{-3}$	$2{,}088 \times 10^{-3}$	$3{,}688 \times 10^{-3}$	$2{,}216 \times 10^{-1}$

9	150	0	$9{,}141 \times 10^{-3}$	$7{,}048 \times 10^{-3}$	$9{,}213 \times 10^{-3}$
10	150	0	$5{,}022 \times 10^{-2}$	$5{,}022 \times 10^{-2}$	$2{,}356 \times 10^{-2}$
11	100	$2{,}223 \times 10^{-3}$	$2{,}223 \times 10^{-3}$	$1{,}194 \times 10^{-3}$	$2{,}343 \times 10^{-2}$

Figure 5 illustrates the dose rate on walls 1, 6, and 7, aligned with the Z-axis. The proton source is located on the Z-axis, where the protons begin to interact with the air until they reach the shield walls at $Z = -2800$ and $Z = -2500$. The protons then interact with the shield walls, and after a certain thickness, they produce dose rate values that comply with regulations. Wall 1, with a thickness of 185 cm, can attenuate radiation to a value of 0.206 μSv/hour. Walls 6 and 7, with a thickness of 350 cm, can attenuate radiation to values of 0.2193 and 2.065 μSv/hour, respectively. Walls 6 and 7 are primary shield walls with high particle flux, requiring a large thickness to effectively attenuate radiation.

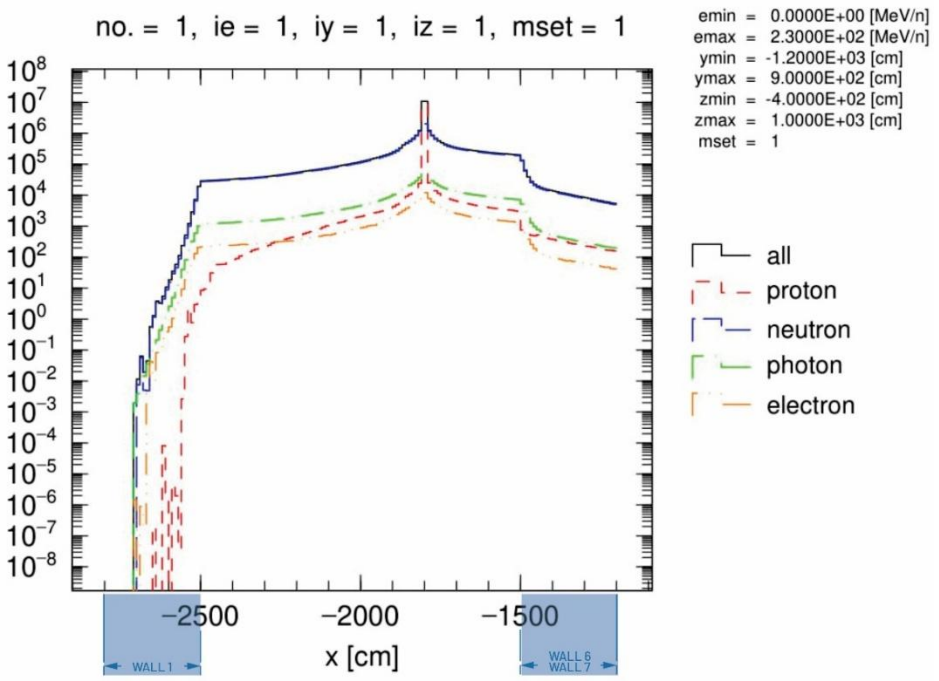

Figure 5. Graph of dose rate on the X-axis of cyclotron room.

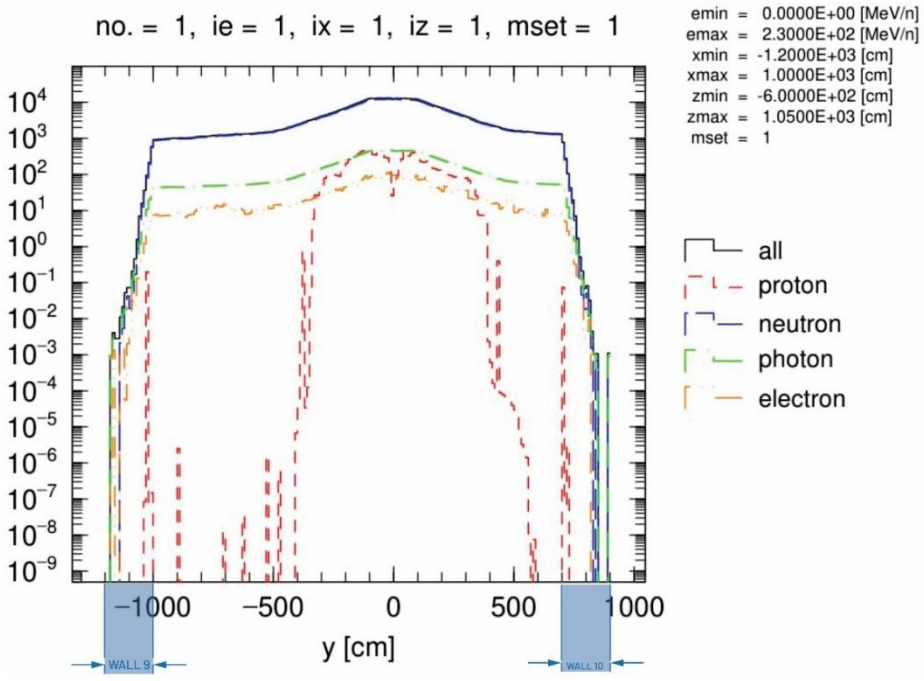

Figure 6. Graph of dose rate on the Y-axis of treatment room 2.

Figure 6 depicts the dose rate on wall 11, which spans the Z-axis range from Z = 1700 to Z = 1900. This wall, with a thickness of 100 cm, is designed to attenuate radiation to a dose rate of 0.0343 μSv/hour. Wall 11 serves as the shielding for the proton therapy treatment room entrance. Given its strategic location, this wall plays a crucial role in minimizing radiation exposure for individuals entering the treatment room. The chosen thickness effectively reduces the radiation levels to meet safety standards, ensuring that the entrance remains safe for both patients and staff.

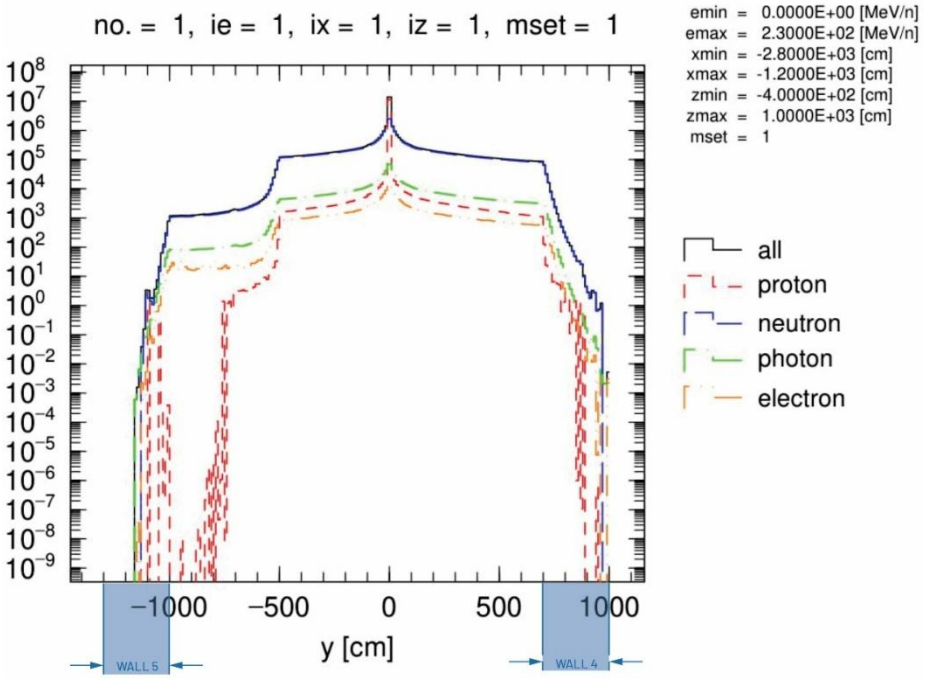

Figure 7. Graph of dose rate on the Y-axis of cyclotron room.

Figure 7 shows the dose rate on walls 4 and 5, with wall 4 covering the Z-axis range from Y = 700 to Y = 1000 and wall 5 spanning Y = 1000 to Y = 1300. Wall 4, with a thickness of 220 cm, effectively attenuates radiation to a dose rate of 0.0856 μSv/hour. On the other hand, wall 5, with a thickness of 170 cm, reduces radiation to a dose rate of 0.0579 μSv/hour. Wall 4 needs to be thicker because it is located closer to the right side of the cyclotron, where radiation levels are higher due to the proximity to the proton source. Wall 5, being farther to the left of the cyclotron, does not require as much shielding thickness, as the radiation intensity decreases with distance from the source. The varying thicknesses of these walls ensure that radiation exposure is minimized in both areas, meeting safety standards for the facility.

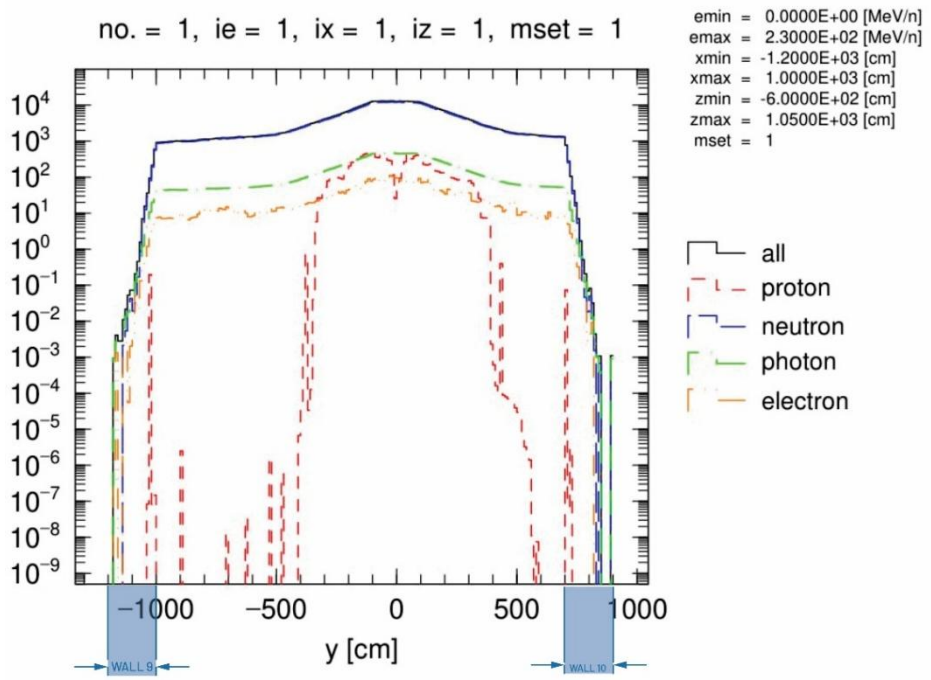

Figure 8. Graph of dose rate on the Y-axis of Treatment room 1.

Figure 8 illustrates the dose rate on walls 9 and 10, with wall 9 covering the Y-axis range from Y = -1200 to Y = -1000. Wall 9, with a thickness of 150 cm, effectively attenuates radiation to a dose rate of 0.009213 μSv/hour. This wall is located in Treatment Room 1, where proton therapy is conducted. Similarly, wall 10, also with a thickness of 150 cm, attenuates radiation to a higher dose rate of 0.02356 μSv/hour.

Wall 10 experiences a higher dose rate attenuation because it is positioned closer to the direction of the proton beam during therapy, where radiation exposure is more intense. Both walls play crucial roles in shielding the treatment rooms, ensuring the safety of patients and staff by reducing radiation exposure to acceptable levels according to safety standards. The varying attenuation levels are accounted for by the different proximities to the proton beam, with wall 10 requiring more shielding due to its closer location to the beam's path.

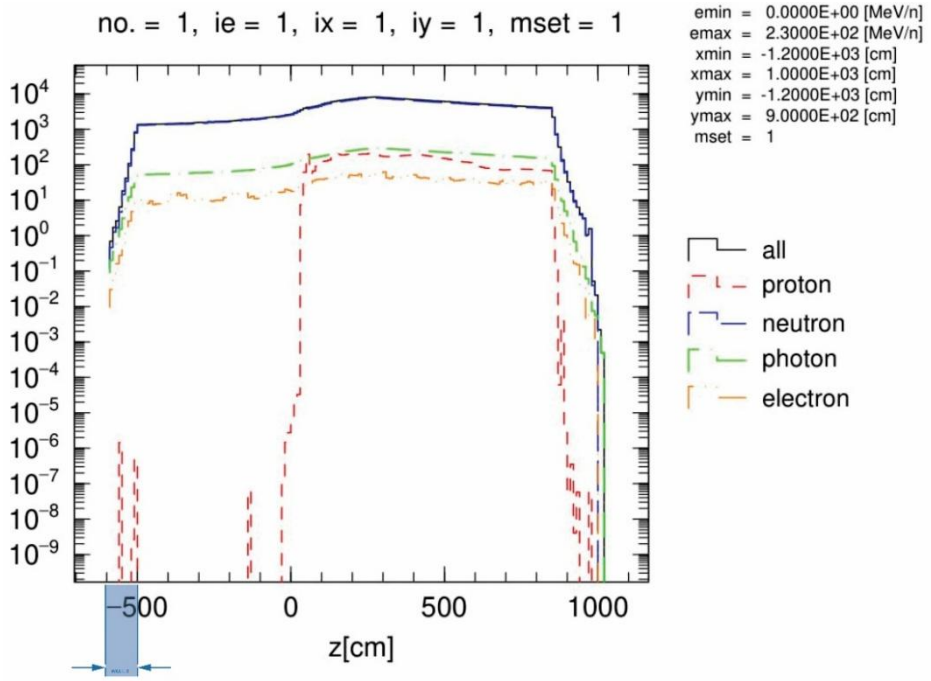

Figure 9. Graph of dose rate on the Z-axis of roof cyclotron room.

Figure 9 presents the dose rate on the ceiling of the cyclotron room, where the shielding has a thickness of 150 cm, effectively attenuating radiation to a dose rate of 0.1544 µSv/hour. Since this is the ceiling, it does not pose a direct risk to people or staff, as there is no one typically present in this area. The ceiling's purpose is mainly to limit radiation exposure to any potential overhead equipment or external areas, ensuring the safety of the facility as a whole. Figure 10 shows the dose rate on the floor of the cyclotron room for wall 2, and the floor of Treatment Room 1 for wall 8, both with a shielding thickness of 200 cm. Wall 2, located in the cyclotron room, can attenuate radiation to a dose rate of 0.1829 µSv/hour. Wall 8, in Treatment Room 1, reduces the dose rate to 0.2216 µSv/hour.

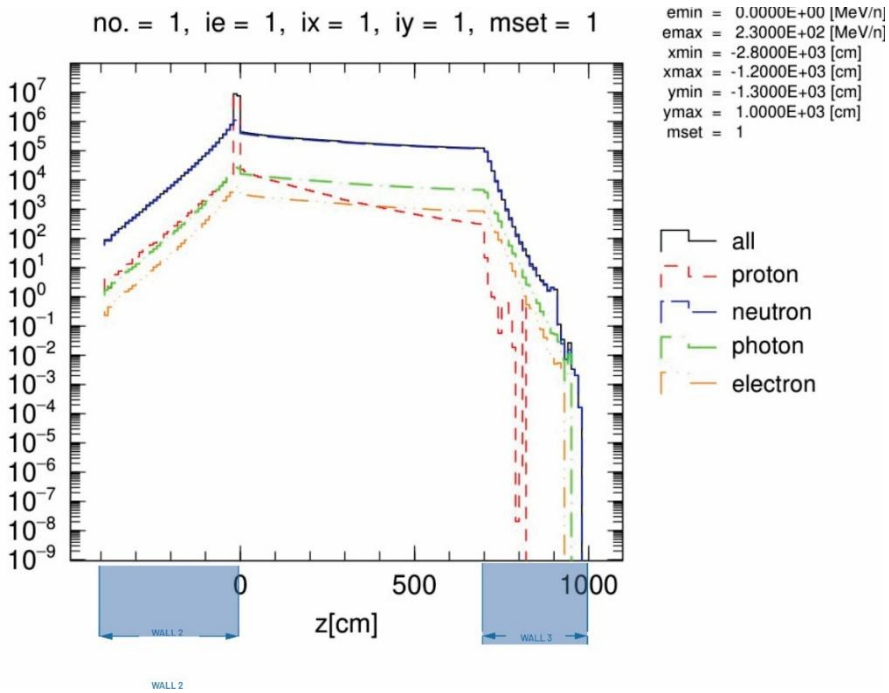

Figure 10. Graph of dose rate on the Z-axis of floor cyclotron room.

Portland cement is the most commonly used shielding material for radiation protection. This preference arises not only from its easy availability in Indonesia—supported by the Indonesian National Standard (SNI)—but also from its cost-effectiveness in large-scale applications. With a density of 2.35 g/cm^3, Portland cement has the lowest density compared to other shielding materials, such as barite or heavy concrete. In addition, it contains relatively few high atomic number (Z) elements, which limits its attenuation capability for high-energy radiation.

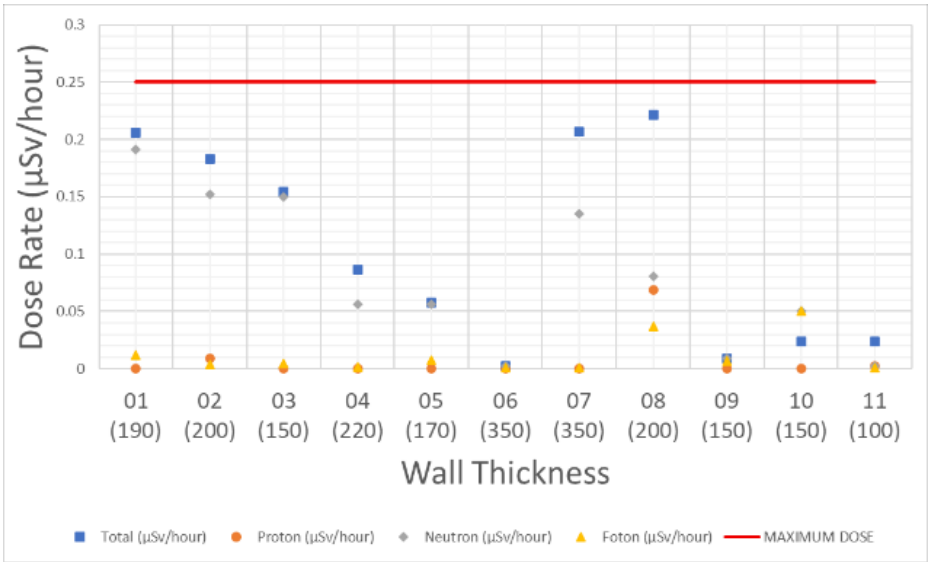

Figure 11. The dose rate graph of the Portland cement shielding design.

The principle of radiation attenuation indicates that materials with higher density and higher atomic number atoms provide better shielding efficiency. As a result, Portland cement requires relatively thicker wall constructions compared to other materials to achieve the same dose reduction. This effect is clearly reflected in the comparison of dose rates across various wall thicknesses, as presented in Figure 11. The figure demonstrates that the total dose rate decreases as the wall thickness increases, with contributions from photons, neutrons, and protons gradually suppressed.

A key observation from the findings is that, while thinner walls (e.g., 100–150 cm) reduce dose rates to some extent, they still approach or slightly exceed safety margins when compared to the BAPETEN maximum dose limit of 0.25 μSv/hour. Conversely, at greater wall thicknesses (e.g., 200–350 cm), the dose rate falls significantly below this regulatory threshold, indicating effective shielding performance. This confirms the strong dependency of dose reduction on wall thickness when using Portland cement.

The optimization process has highlighted an important trade-off between material efficiency and radiation safety. Although thicker walls ensure compliance with BAPETEN regulations, excessive thickness leads to higher construction costs and space limitations. From the analysis, an optimized wall thickness in the range of 200–220 cm provides a reliable balance—achieving dose rates well under the maximum dose while minimizing unnecessary increases in material usage. This optimized design ensures both safety compliance and practical efficiency, reinforcing the suitability of Portland cement as a feasible radiation shielding material in Indonesia.

CONCLUSION

Based on the measurements of wall thickness and the radiation dose rate provided in the table and graph, it can be concluded that the radiation protection in the proton therapy room with 230 MeV energy is within safe limits. The total radiation dose detected at all tested wall thicknesses, which range from Wall 1 (190 cm) to Wall 11 (100 cm), remains below the threshold value recommended by BAPETEN, which is 0.25 μSv/hour. No dose rate exceeds this value for any of the wall thicknesses, indicating that the radiation protection applied in the proton therapy room is effective in reducing radiation exposure. Therefore, it can be concluded that the proton therapy room meets the radiation safety standards and poses no significant risk to personnel in the surrounding area.

While this study demonstrates the effectiveness of the concrete walls, further research is highly recommended to explore the use of alternative or composite shielding materials that could offer comparable or superior protection with thinner walls and lower costs, potentially optimizing the design of future proton therapy rooms.

AUTHOR CONTRIBUTIONS

D.A.S., M.S., and A.T.O. designed the conceptualization, methodology, simulation, and writing-original manuscript preparation. A.T.O. and Y. S. performed the formal analysis. Y.S., G.S.W., and I.M.T. performed the validation.

CONFLICT OF INTEREST

The authors declare that they have no conflicts of interest.

REFERENCES

Baumann, B.C., Mitra, N., Harton, J.G., Xiao, Y., Wojcieszynski, A.P., Gabriel, P.E., Zhong, H., Geng, H., Doucette, A., Wei, J., O'Dwyer, P.J., Bekelman, J.E. & Metz, J.M. (2020). Comparative effectiveness of proton vs photon therapy as part of concurrent chemoradiotherapy for locally advanced cancer. *JAMA Oncology*, 6(2), 237-246. https://doi.org/10.1001/jamaoncol.2019.4889

Brodin, N.P., Kabarriti, R., Schechter, C.B., Pankuch, M., Gondi, V., Kalnicki, S., Garg, M. K., & Tome, A. (2021). Individualized quality of life benefit and cost-effectiveness estimates of proton therapy for patients with oropharyngeal cancer. *Radiation Oncology*, 16(19), 1-9. https://doi.org/10.1186/s13014-021-01745-1

Caffrey, J.A., 2017. *Radiation shielding for space nuclear propulsion*. Oregon State University.

Chen, Z., Dominello, M.M., Joiner, M.C. & Burmeister, J.W. (2023). Proton versus photon radiation therapy: A clinical review. *Frontier in Oncology*, 13 (2023), 1-28. https://doi.org/10.3389/fonc.2023.1133909

Chen, Z.P., Zhang, Z.Y., Xie, J.S., Guo, Q., & Yu, T. (2019). Metaheuristic optimization method for compact reactor radiation shielding design based on genetic algorithm. *Annals of Nuclear Energy*, 134 (1), 318–329. https://doi.org/10.1016/j.anucene.2019.06.031

Depuydt, T. (2018). Proton therapy technology evolution in the clinic: impact on radiation protection. *Annals of the ICRP*, 47(3-4), 177-186. https://doi.org/10.1177/0146645318756252

Detwiler, R.S., McConn, R.J., Grimes, T.F., Upton, S.A. & Engel, E.J. (2021). *Data Mining Analysis and Modeling Cell: Compendium of Material Composition Data for Radiation Transport Modeling*. Homeland Security. United States of America. https://doi.org/10.2172/1782721

Durante, M. & Cucinotta, F. A. (2011). Physical basis of radiation protection in space travel. *Reviews of Modern Physics*, 83, 1245–1281. https://doi.org/10.1103/RevModPhys.83.1245

El-Genk, M.S. (2009). Deployment history and design considerations for space reactor power systems. *Acta Astronaut*. 64, 833–849. http://dx.doi.org/10.1016/j.actaastro.2008.12.016

Garg, T. & Shrigiriwar, A. (2022). Radiation Protection in Interventional Radiology. *Indian Journal of Radiology and Imaging*, 31(4), 939-945. https://doi.org/10.1055/s-0041-1741049

Giménez, M.A.N. & Lopasso, E.M. (2018). Tungsten carbide compact primary shielding for small medium reactor. *Annals of Nuclear Energy,* 116, 210–223. https://doi.org/10.1016/j.anucene.2018.02.032

Goitein, M. (1985). Calculation of the uncertainty in the dose delivered during radiation therapy. *Medical Physics,* 12(5), 608-612. https://doi.org/10.1118/1.595762

Gultom, R.H.A. (2024). *Studi Variasi Jenis Material Perisai Radiasi pada Ruang Siklotron 230 MeV 300 nA untuk Fasilitas Terapi Proton menggunakan Program PHITS*. Universitas Gadjah Mada. Indonesia

Huang, D., Frank, S.J., Verma, V., Thaker, N.G., Brooks, E.D., Palmer, M.B., Harrison, R.F., Deshmukh, A.A. & Ning, M.S. (2021). Cost-Effectiveness Models of Proton Therapy for Head and Neck: Evaluating Quality and Methods to Date. *International Journal of Particle Therapy*, 8(1), 339-353. https://doi.org/10.14338/ijpt-20-00058.1

Krishnaraja, A.R. & Guru, K.V. (2021). 3D Printing Concrete: A Review. *IOP Conference Series: Materials Science and Engineering*. 1055. 012033. https://doi.org/10.1088/1757-899X/1055/1/012033

Matsumoto, S., Koba, Y., Kohno, R., Lee, C., Bolch, W.E. & Kai, M. (2016). Secondary Neutron Doses to Pediatric Patients During Intracranial Proton Therapy: Monte Carlo Simulation of the Neutron Energy Spectrum and its Organ Doses. *Health Physics*, 110(4), 380-6. https://doi.org/10.1097/hp.0000000000000461

Penfold, S.N. (2022). Radiation shielding assessment of high-energy proton imaging at a proton therapy facility. *Medical Phys*ics, 49(8), 5340-5346. https://doi.org/10.1002/mp.15727

Penfold SN. (2022). Radiation shielding assessment of high-energy proton imaging at a proton therapy facility. *Medical Physics*, 49(8), 5340-5346. https://doi.org10.1002/mp.15727

Popov, A.L., Kolmanovich, D.D., Chukavin, N.N., Zelepukin, I.V., Tikhonowski, G.V., Pastukhov, A.I., Popov, A.A., Shemyakov, A.E., Klimentov, S.M., Ryabov, V.A., Deyev, S.M., Zavestovskaya, I.N. & Kabashin, A.V. (2024). Boron Nanoparticle-Enhanced Proton Therapy: Molecular Mechanisms of Tumor Cell Sensitization. *Molecules*, 29(16), 3936. https://doi.org/10.3390/molecules29163936

Ramoisiaux, E., Hernalsteens, C., Tesse, R., Gnacadja, E., Pauly, N., Vanwelde, M. & Stichelbaut, F. (2023). Concrete shielding activation for proton therapy systems using BDSIM and FISPACT-II. *Journal of Physics: Conference Series*, 2420, 012064. https://doi.org/10.1088/1742-6596/2420/1/012064

Reistad, O. & Ølgaard, P.L. (2006). *Russian Nuclear Power Plants for Marine Applications*. Norwegian Radiation Protection Authority, Norway.

Ruth, T. (2009). Accelerating production of medical isotopes. *Nature,* 457, 536–537. https://doi.org/10.1038/457536a

Saadi, M.K. & Moadab, N.H. (2019). Optimization of an Am-Be neutron source shield design by advanced materials using MCNP code. *Radiation Physics and Chemistry,* 158, 109–114. https://doi.org/10.1016/j.radphyschem.2019.01.026

Shang, Y., Yang, G., Su, G., Feng, Y., Ji, Y., Liu, D., Yin, R., Liu, C., & Shen, C. (2020). Multilayer polyethylene/hexagonal boron nitride composites showing high neutron shielding efficiency and thermal conductivity. *Composites Communications,* 19, 147-153. https://doi.org/10.1016/j.coco.2020.03.007

Tabbakh, F., Hosmane, N.S., Tajudin, S.M., Ghorasi, A., & Morshedian, N. (2022). Using 157Gd doped carbon and 157GdF4 nanoparticles in proton-targeted therapy for effectiveness enhancement and thermal neutron reduction: a simulation study. *Scientific Reports*, 12, 17404. https://doi.org/10.1038/s41598-022-22429-0

Till, J.E. & Grogan, H.A. (2008). *Radiological Risk Assessment and Environmental Analysis*. Oxford: Oxford University Press. https://doi.org/10.1093/acprof:oso/9780195127270.001.0001

Yamaji, A. & Sako, K. (1994). Shielding design to obtain compact marine reactor. *Journal of Nuclear Science and Technology*. 31 (6), 510–520. https://doi.org/10.1080/18811248.1994.9735185

Wan, H., Xu, Z., Shao, J. Sun, Z., Li, L. & Wu, X. (2017). Primary design and optimization of shielding for nuclear medical ship reactor. *High Power Laser and Particle Beams*, 29 (1), 1–4. https://doi.org/10.11884/HPLPB201729.160235